Int. J. Electrochem. Sci., 9 **(2014)** 6438 - 6450

International Journal of
ELECTROCHEMICAL
SCIENCE
www.electrochemsci.org

Electrodeposition of Nanocrystalline Ni-Mo Alloys from Alkaline Glycinate Solutions

Yahia H. Ahmad[1], *A.M.A. Mohamed*[1,*], *Teresa D. Golden*[2], *Nandika D'Souza*[3]

[1] Center of Advanced Materials, 2713, Qatar University, Doha, Qatar
[2] University of North Texas, Department of Chemistry, 1155 Union Circle #305070, Denton, TX 76203, USA
[3] University of North Texas, Department of Materials Science and Engineering, Denton, TX 76207, USA
[*]E-mail: adel.mohamed@qu.edu.qa

Received: 15 May 2014 / *Accepted:* 16 June 2014 / *Published:* 25 August 2014

The induced electrodeposition of nanocrystalline Ni-Mo alloys was investigated using two different molar ratios of Ni:Mo in sodium glycinate solution at pH 9.3. The chemical nature of the Ni^{2+} and MoO_4^{2-} in alkaline glycinate solution was studied using UV-Vis absorption spectroscopy. The composition of the coating layer was determined using EDX. The crystallinity of electrodeposits was examined using XRD, whereas, the morphology and topography were investigated using SEM and AFM, respectively. The corrosion resistance of Ni-Mo alloys compared to pure Ni was studied in 3.5 % NaCl solution using potentiodynamic polarization and electrochemical impedance techniques. Ni-Mo alloy electrodeposited from the solution containing $[MoO_4^{2-}]/[Ni^{2+}]$ molar ratio of 0.2 show higher corrosion resistance compared to plating solutions of molar ratio 0.1 and pure Ni.

Keywords: Ni-Mo alloy; electrodeposition; alkaline glycinate solution; corrosion

1. INTRODUCTION

Molybedenum and its alloys are of great importance due to wide range of applications especially in electrochemistry due to high catalytic activity. They are used as catalysts in hydrogen and oxygen evolution reactions [1, 2], as well as catalysts for hydroprocessing of aromatic oils and gas phase hydrogenation of benzene [3]. Pure molybdenum cannot be produced by electrodeposition from aqueous solutions but it can be codeposited with an iron group metal which is known as induced electrodeposition [4].

Among different alloys of molybdenum, Ni-Mo alloys are of great interest due to their high corrosion resistance and low overpotential for the hydrogen evolution reaction. The preparation of Ni-

Mo alloys by metallurgical methods was found to be inconvenient due to oxidation during the crystallization step and high melting point of molybdenum [5]. Other methods were utilized such as powder metallurgy and mechanical alloying [6, 7], spark plasma sintering [8] and electrodeposition [9-12]. Many studies investigated the electrodeposition of Ni-Mo alloys [5, 13-16]. It was reported that the deposition of Ni-Mo alloys from aqueous solutions containing only Ni^{2+} and MoO_4^{2-} is not possible without using the proper complexing agent due to the formation of the multimolecular heteropolymolybdate $(NiMo_6O_{24}H_6^{4-})_n$ complexes which are very difficult to reduce [17]. The electrodeposition of Ni-Mo was tried from electrolytes of different complexing agents e.g. acetate, tartarate, pyrophosphate, citrate and ammonia but only citrate and pyrophosphate seem to be the most promising with respect to quality, adhesion and mechanical properties [5, 18].

Glycine has been used as a complexing agent in the electrodeposition of many binary metallic alloys like Zn-Ni [19], Cu-Co [20] and Zn-Co [21]. In addition to the buffering action of glycine in the electrodeposition process, it was found that deposition from alkaline glycinate baths give rise to high quality deposits and high deposition rates [22]. The aim of the present work was undertaken to investigate the electrodeposition of Ni-Mo alloys from alkaline glycinate solutions (pH 9.3), to study the crystalline orientation, morphology and corrosion resistance of the electrodeposited Ni-Mo alloys compared to pure Ni.

2. EXPERIMENTAL

Ni-Mo alloys were electrodeposited from alkaline glycinate solutions under galvanostatic conditions. The bath composition and electrolysis parameters for the electrodeposition process are listed in Table 1. The electrolytic bath was composed of 0.1 M $NiSO_4.7H_2O$ (BDH), 0.4 M sodium glycinate (BDH), 0.15 g/l saccharin (Merck) and variable concentrations of $Na_2MoO_4.2H_2O$ ranging from 0.01-0.05 M (BDH). All of the electrolytic solutions were prepared using deionized water.

Table 1. Bath composition for electrodeposition of Ni-Mo alloy.

Solution composition	
Electrolyte	
$NiSO_4.7H_2O$	0.1 M
$Na_2MoO_4.2H_2O$	0.01-0.05 M
Sodium glycinate	0.4 M
Saccharin	0.15 g/l
Electrodeposition conditions	
pH	9.3
Temperature	20 °C
Electrolyte agitation	Magnetic stirring 250 rpm
Cathode	Carbon steel sheet (area 2.0 cm^2)
Anode	Ni foil (area 16 cm^2)
Current density	5 A dm^{-2}
Quantity of charge	160 C cm^{-2}

Analytical grade carbon steel sheets were used as the cathode (area 2.0 cm^2) which were mechanically polished, sonicated for 10 minutes in water and dried in air before immersion in the test solution. During electrodeposition the bath temperature was kept at 20 °C and the initial pH was adjusted at 9.3 by addition of sodium hydroxide solution. Nickel sheet of 99.9 % purity (BDH) was used as the anode and saturated calomel electrode was used as a reference electrode.

Electrodeposition of nanocrystalline Ni-Mo alloys was carried out under galvanostatic conditions at a current density of 5 A dm^{-2} using Bio-Logic EC-Lab potentiostat/galvanostat version 10.2.

The preferred crystalline orientation of Ni was examined by X-ray diffraction (XRD) technique utilizing a Miniflex II X-ray diffractometer (Rigaku Corporation, Japan) at 30 kV voltage, 15 mA current, 0.3 mm receiving slit, and using Cu-Kα radiation.

Visible absorption spectra were measured using Perkin Elmer double beam spectrophotometer (Lambda 25). Two matched quartz cells with bath length of 1 cm were used; one for the blank solution and the second for the sample. All measurements were performed in the wavelength range of 300-1000 nm with 1 nm intervals.

The microstructure of the coatings was studied by scanning electron microscopy (SEM) and recorded with a Nova NanoSEM 450 FEI, (Netherlands), whereas, the composition of metallic coatings was analyzed using energy dispersive X-ray spectroscopy (EDX).

The surface topography and heterogeneities of Ni-Mo coating layers were examined by an Atomic Force Microscopy (AFM). Measurements were performed under ambient conditions using the Standard Topography AC air (tapping mode in air). An AFM head scanner applied with Si cantilever adjacent vertically in the sample resonant frequency of the free-oscillating cantilever set as the driving frequency.

Corrosion behavior of Ni-Mo films was investigated in 3.5 % NaCl solution using Tafel polarization and electrochemical impedance spectroscopy. The potentiodynamic polarization studies have been configured into a three-electrode cell consisting of SCE as a reference electrode, Pt gauze as a counter electrode and the coating layer as a working electrode. The potentiodynamic scan was carried out in the range -250 mV to + 250 mV versus the open-circuit potential with a scan rate of 0.1 mV s^{-1} in naturally aerated solutions at room temperature 293K. The electrochemical impedance spectroscopy (EIS) investigations were carried out using input signal 10 mV peak to peak in the frequency domain 0.1-10^5 Hz.

3. RESULTS AND DISCUSSION

3.1. Absorption spectroscopy

Visible absorption spectra of Ni(II)-MoO_4^{2-}-glycinate baths were studied in order to get more information about the complexation between Ni^{2+}, MoO_4^{2-} and glycinate ion. Fig. 1 presents the spectra of solutions containing different molar ratios of glycinate in the range 350-1000 nm at pH 9. The spectra show two absorption bands in the studied range due to d-d transitions of the complex species between Ni^{2+} and glycinate ions; the first band at 300-500 nm and the second at 500-850 nm. A third peak starts at 850 nm to high wavelengths out of the studied wavelength range. It may be

observed that the increasing in the concentration of glycinate ions led to a shift in the peaks maxima toward the lower values of wavelength and decreasing in the peak intensity compared to glycinate-free solution. This shift in the peak maxima and the intensities is attributed to the change in the stoichiometry of the complexes formed by interaction of glycinate ions with Ni^{2+} and MoO_4^{2-} [23, 24].

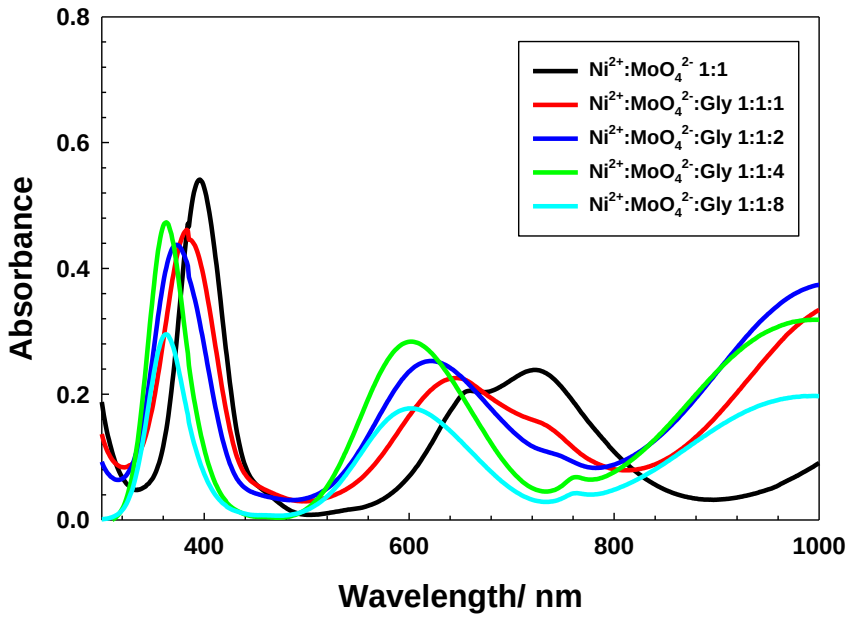

Figure 1. Absorption spectra of Ni^{2+}-MoO_4^{2-}-glycinate baths containing different molar ratios of glycinate at wavelength 300-1000.

3.2. Cyclic Voltammetry studies

The cyclic voltammograms of solutions containing pure Ni^{2+}, Ni^{2+}:MoO_4^{2-} 10:1 and Ni^{2+}:MoO_4^{2-} 5:1 at a sweep rate of 50 mV s^{-1} are presented in Fig. 2.

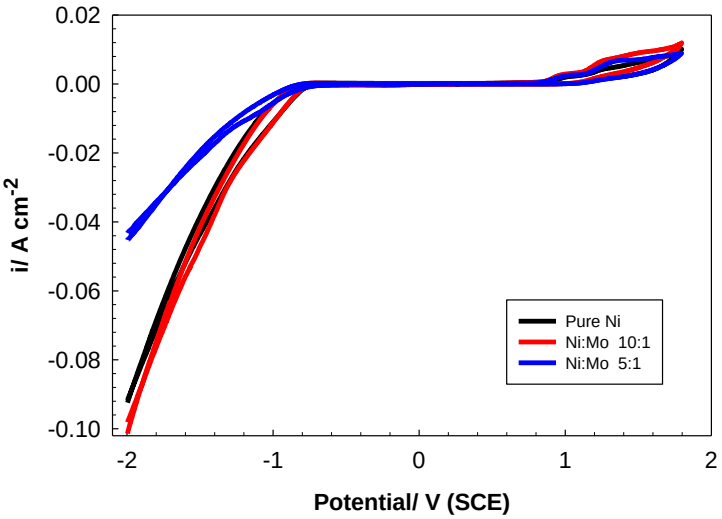

Figure 2. The cyclic voltammograms of pure Ni and the two Ni-Mo alloys.

The voltammetric response shows no significant difference between different solutions. It may also be observed that no peaks appear in the cathodic range prior to hydrogen evolution which confirm that Ni^{2+} and MoO_4^{2-} reduction to form Ni and Ni-Mo metallic coating takes place simultaneously with the hydrogen evolution reaction. It was suggested that molybdate reduction proceeded first with the formation of Mo (IV) oxide as an intermediate which is consequently reduced to molybdenum in the alloy especially under the catalytic action of Ni atoms [25].

3.3. Crystalline orientation

Figure 3 shows the XRD patterns of pure Ni and different Ni-Mo coatings. The XRD spectrum of pure Ni shows that (111) is the preferred crystalline orientation with the presence of secondary lower intensity peaks for (200), (220), (400), (311) and (222) as shown in Fig. 3(A).

Table 2. XRD reflections for pure Ni and different types of Ni-Mo metallic coatings.

Crystalline Orientation (hkl)	Pure Ni		Ni:Mo 10:1		Ni:Mo 5:1	
	d (Å)	$[I]/[I_0]$	d (Å)	$[I]/[I_0]$	d (Å)	$[I]/[I_0]$
111	2.0274	100	2.0002	100	1.9969	100
200	1.7795	53	1.7534	46	1.7155	45
220	1.2437	47	1.2412	43	1.2398	40
400	1.1692	41	1.1629	50	1.1616	51
311	1.0577	43	1.0456	46	1.0401	51
222	1.0113	42	1.0091	47	1.0082	50

The XRD patterns of pure Ni and Ni-Mo alloys and the relative intensities of the reflection lines (Table 2) confirms the presence of different phases in case of Ni-Mo 10:1 and 5:1 alloys i.e. nanocrystalline Ni-Mo alloy dispersed in pure Ni phase.

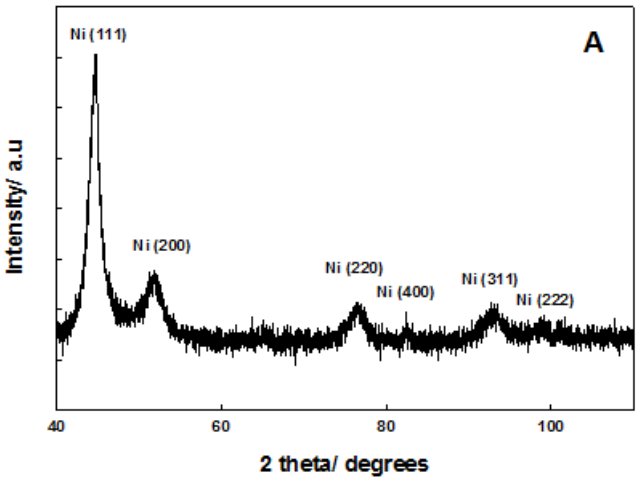

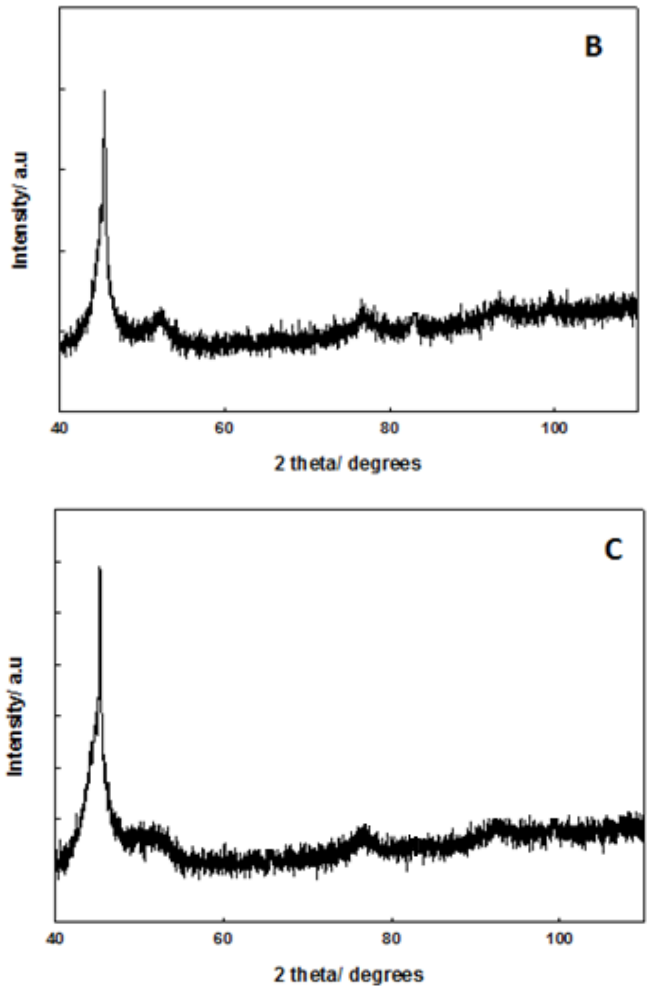

Figure 3. XRD patterns of: A) pure Ni, B) Ni:Mo 10:1 and C) Ni:Mo 5:1.

3.4. Potentiodynamic polarization measurements

Fig. 4 illustrates the Tafel polarization curves of pure Ni and Ni-Mo coatings after 24h immersion in 3.5% NaCl solution. The values of calculated corrosion parameters are listed in Table 3.

Table 3. Corrosion parameters of pure Ni and Ni-Mo coatings after 24h in 3.5% NaCl at 20 °C.

Sample type	E_{Corr} (mV)	I_{Corr} (μA cm^{-2})	β_a (V $decade^{-1}$)	β_c (V $decade^{-1}$)	R_p (kΩ cm^2)
Ni	-415	$4.3x10^{-6}$	0.236	0.218	11.44
Ni:Mo 10:1	-384	$1.52x10^{-6}$	0.210	0.122	22.04
Ni:Mo 5:1	-374	$4.51x10^{-7}$	0.140	0.136	66.24

According to the obtained data the corrosion potential, E_{corr} is shifted to less negative values as the Mo content of the metallic coating increases. The corrosion current density, i_{corr} decreases from $4.3x10^{-6}$ A cm^{-2} for pure Ni to $1.52x10^{-6}$ and $4.51x10^{-7}$ A cm^{-2} for Ni:Mo 10:1 and Ni:Mo 5:1, respectively. Equation (1) was used to calculate the polarization resistance, R_p:

$$R_p = \frac{(\beta_a.\beta_c)}{2.303 i_{Corr}(\beta_a+\beta_c)} \quad (1)$$

where i_{corr} is the corrosion current density, R_p is the polarization resistance and β_a, β_c are the anodic and cathodic Tafel slopes, respectively. The electrocatalytic activity of Ni-Mo films for hydrogen evolution has been shown by others [26, 27]. Beginning at a lower potential, an increase in the cathodic current is seen for the Ni-Mo coating containing a higher percentage of Mo. Halim et. al. has shown that Mo percentage and surface roughness are the main factors for increasing hydrogen evolution reaction [28]. For the anodic branch a wider passive region can be obtained showing the influence of the Mo in the Ni-Mo alloy. The Mo influences the anodic dissolution reaction in the pitting region by enhancing the growth of the passive oxide film. This behavior can be seen by the longer passivation region and lower current plateau for the Ni:Mo 5:1 coating anodic scan.

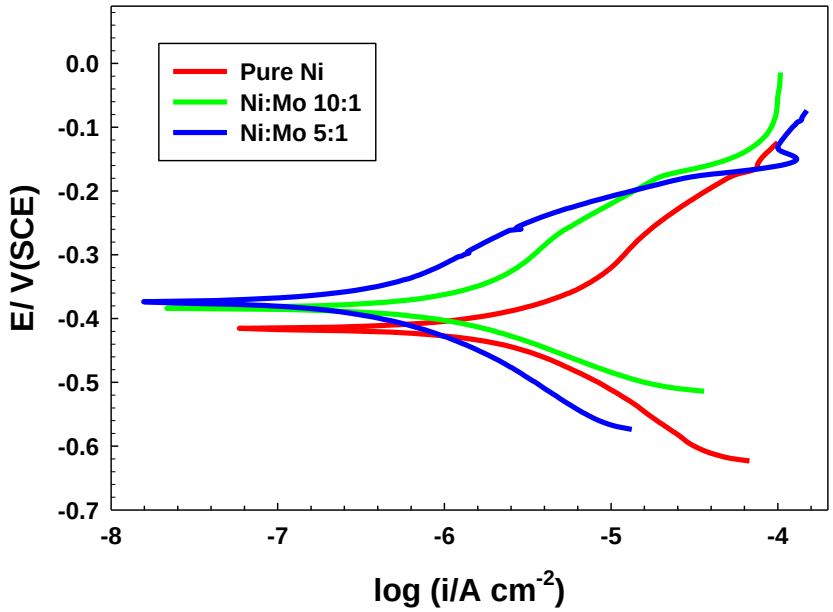

Figure 4. Tafel polarization curves of pure Ni and Ni-Mo coatings.

It was observed that, the R_p values of Ni:Mo 10:1 and Ni:Mo 5:1 increased by 92.66% and 479%, respectively, compared to the R_p value of pure Ni. It may be concluded that the increase in the percentage of Mo in the metallic coating layer facilitates the passivation process of the surface and hence increases the corrosion resistance of the metallic film.

3.5. EIS measurements

The corrosion performance of the different types of coatings including metallic type can be evaluated from the EIS studies. The EIS technique does not disturb the double layer at the metal/solution interface [29, 30]. Fig. 5a represents Bode impedance plots of pure Ni, Ni:Mo 10:1 and Ni:Mo 5:1 coatings after 24h of immersion in 3.5% NaCl solution. Bode plots are recommended as standard impedance plots, since all impedance data are equally represented and the phase angle, θ, is a

sensitive parameter for any surface changes [31, 32]. The broadness of the phase maximum, θ_{max}, shows that the process occurring on the metallic surface is not controlled by one time constant.

Nyquist plots of different films show semicircles of increasing diameter from pure Ni to Ni:Mo 5:1 which means that the increasing in the content of Mo in the metallic coating layer led to an increase in the total impedance value $|Z|$, as shown in Fig. 5(b).

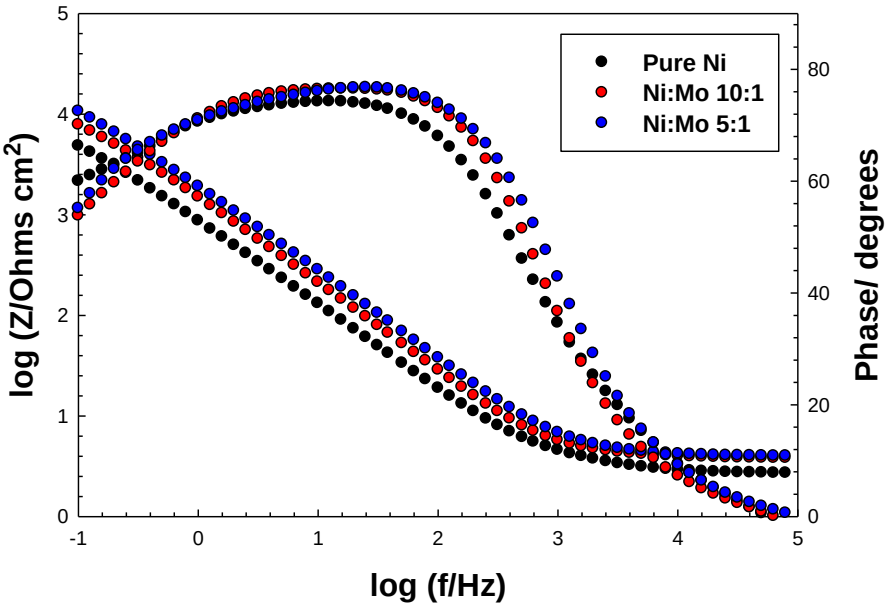

Figure 5a. Bode impedance plots of pure Ni and Ni-Mo films.

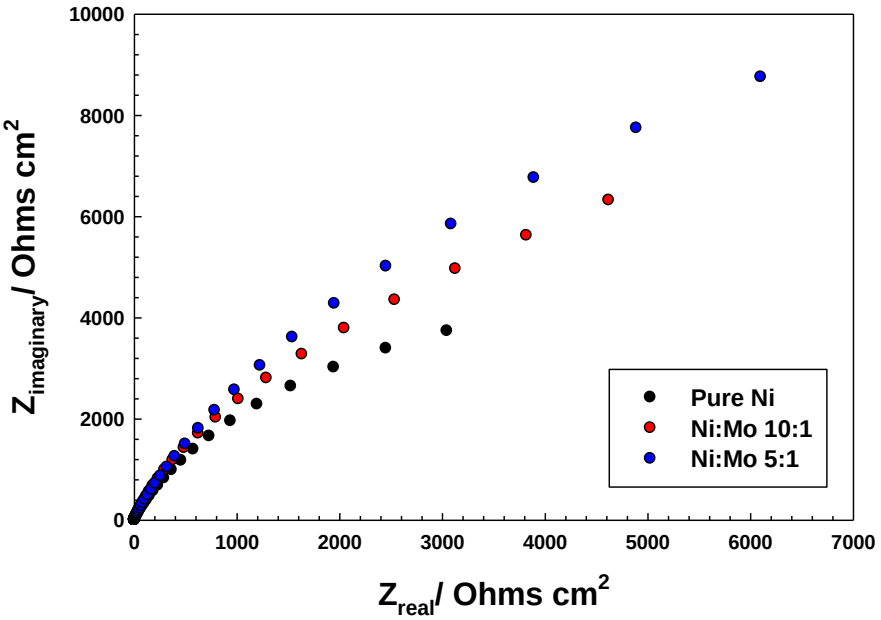

Figure 5b. Nyquist impedance plots of pure Ni and Ni-Mo alloys.

The impedance data were analyzed using software provided with the electrochemical workstation and fitted to theoretical data according to the equivalent circuit model presented in Fig. 6.

Fitting procedures have shown that good agreement between the theoretical and experimental data is obtained if a frequency-dependent constant phase element (CPE) is introduced instead of pure capacitor. The impedance associated with the capacitance of the CPE is a combination of properties related to both the surface and the electroactive species and is described by the equation (2):

$$Z_{CPE} = Y_0^{-1}(j\omega)^{-\alpha} \quad (2)$$

where Y_0 is the frequency independent real constant of the CPE which is identical to the idealized capacitance at ω=1, ω being the angular frequency (ω=2πf), j=√-1, and α is an adjustable empirical exponent varies between 1.0 for a purely capacitive behavior associated with a perfectly smooth surface and 0.5 for a porous electrode [33].

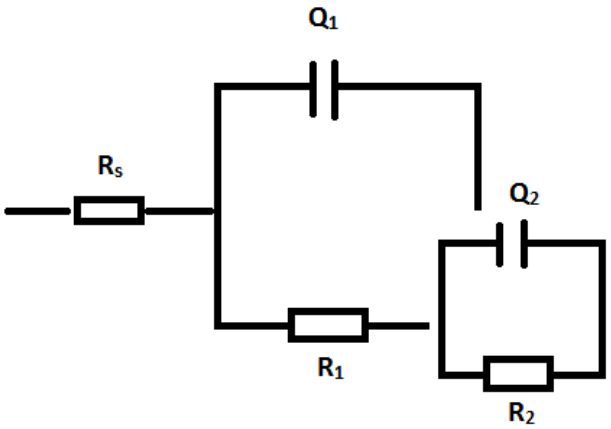

Figure 6. Equivalent circuit model representing electrode/electrolyte interface of different metallic coatings.

Table 4. Equivalent circuit parameters of pure Ni and Ni-Mo alloys after 24h immersion in 3.5 % NaCl solution at 20 °C.

Sample type	R_s (Ω cm^2)	R_1 (Ω cm^2)	Q_1 (Ω^{-1} s$^{\alpha}$ cm^{-2})	α_1	R_2 (kΩ cm^2)	Q_2 (Ω^{-1} s$^{\alpha}$ cm^{-2})	α_2
Pure Ni	2.689	6.231	194.7×10^{-6}	0.83	10.66	53.29×10^{-6}	0.71
Ni:Mo 10:1	3.822	20.03	133.9×10^{-6}	0.87	15.41	22.77×10^{-6}	0.64
Ni:Mo 5:1	3.973	25.36	93.0×10^{-6}	0.87	23.62	12.79×10^{-6}	0.58

The discrepancy between experimental data and theoretical fit is about 2%. The calculated equivalent circuit parameters are listed in Table 4. The equivalent circuit model consists of two circuits R_1Q_1 and R_2Q_2 in parallel combination and their combination is in series with R_s. In this model, R_s, represents the electrolyte resistance, Q_1 is the double layer capacitance and R_1 is the charge transfer resistance. R_2Q_2 combination can be attributed to the passive layer of the metallic coating layer. From the values obtained in Table 4, it is clear that the values of R_2 increases with increasing the Mo content in the metallic film.

3.6. Surface morphology and topography

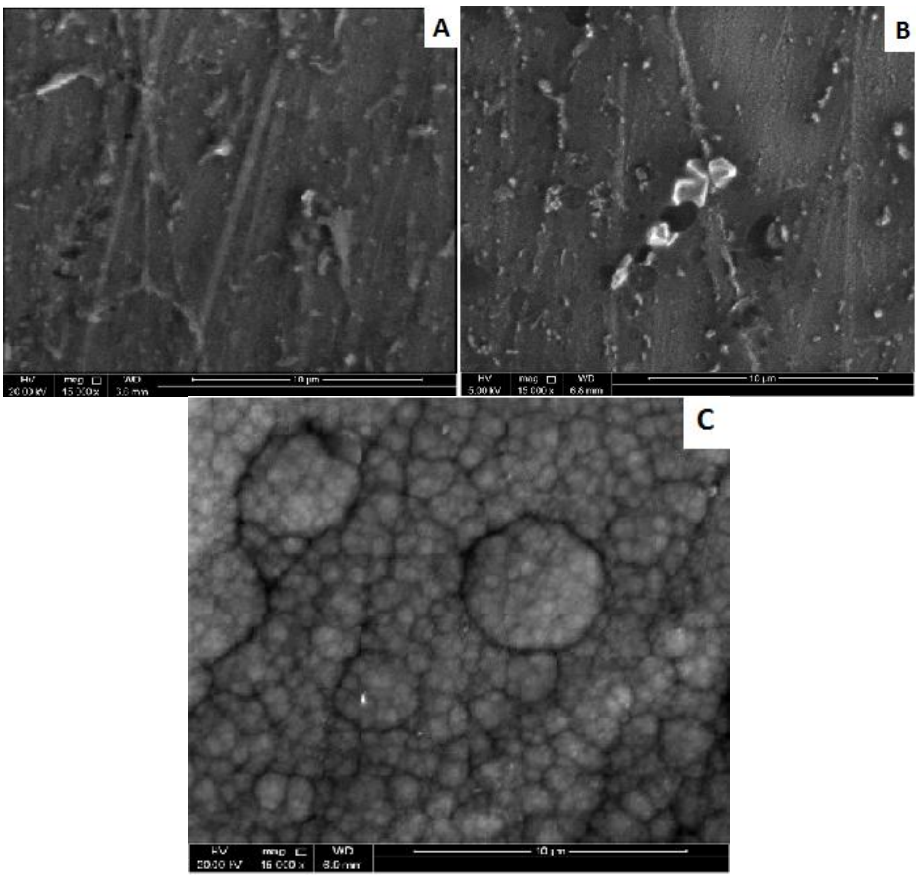

Figure 7. SEM micrographs of: A) pure Ni, B) Ni:Mo 10:1 and C) Ni:Mo 5:1.

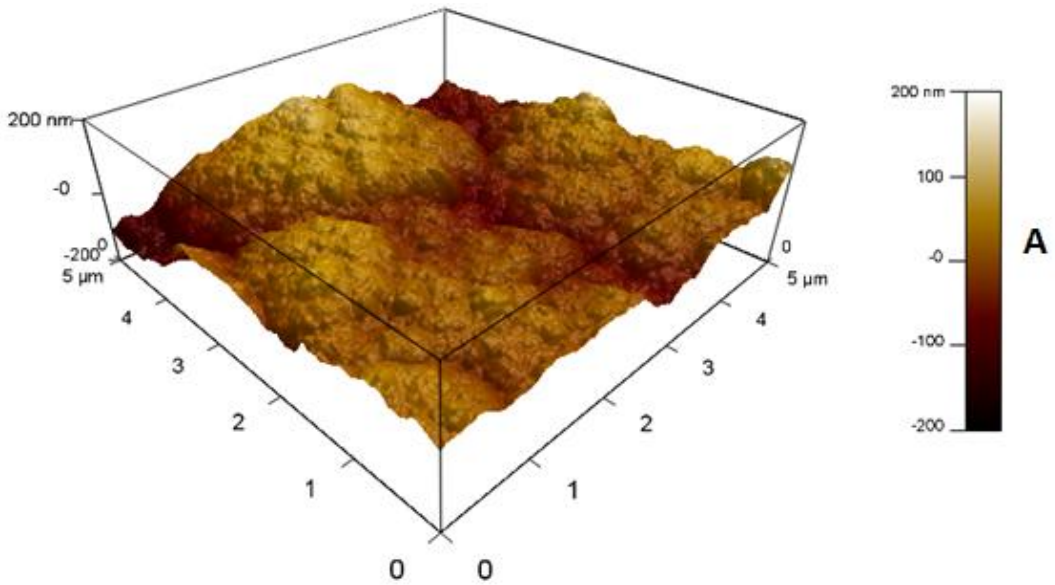

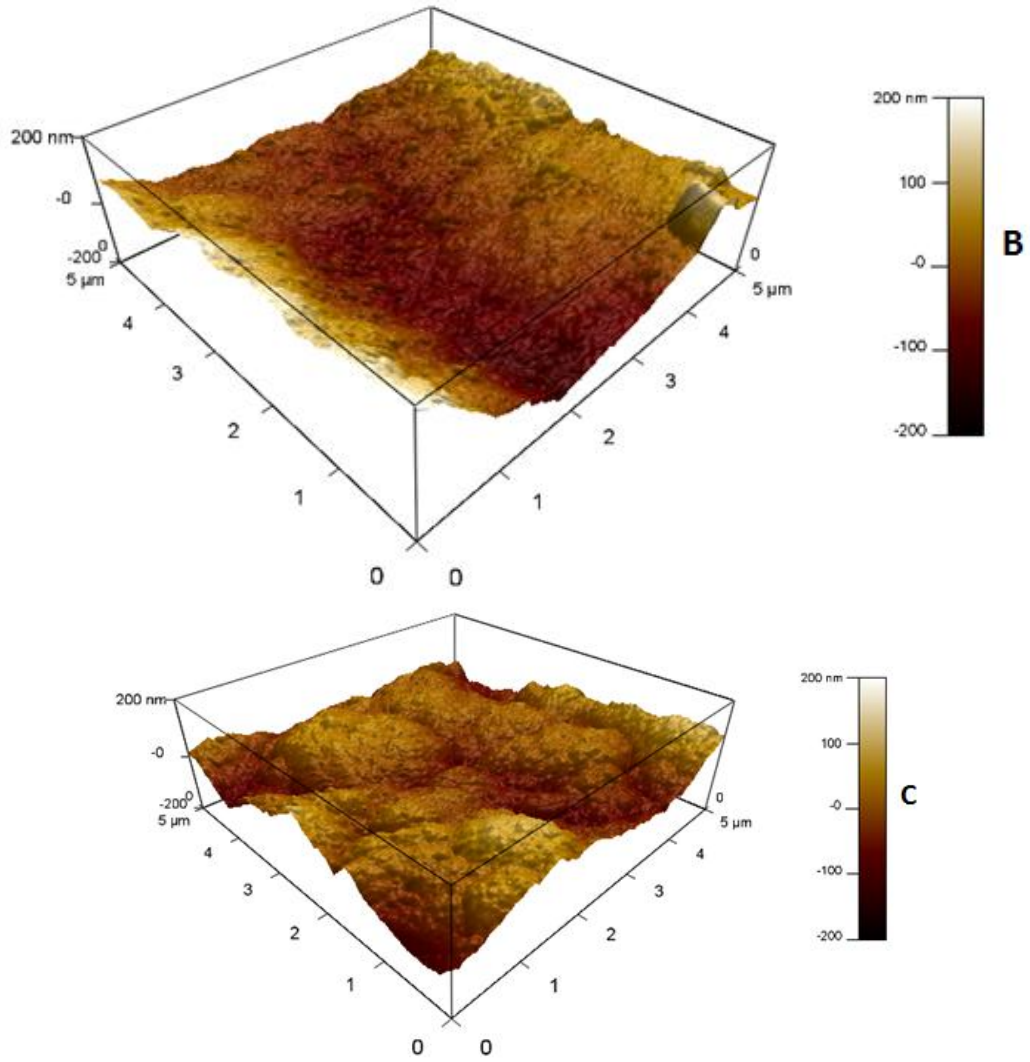

Figure 8. AFM micrographs of: A) pure Ni, B) Ni:Mo 10:1 and C) Ni:Mo 5:1.

Figure 7 shows the scanning electron images of pure Ni and the two Ni-Mo coatings. The micrographs of pure Ni and Ni:Mo 10:1 show compact film and relatively smooth surface while in case of Ni:Mo 5:1 the grains are aggregated in the form of clusters and the surface homogeneity significantly decreases.

The composition of Ni-Mo alloys formed were analyzed using EDX analysis, as listed in Table 5. The elemental composition of Ni-Mo metallic coatings shows the presence of oxygen which is in coincident with the consumption of the formation of Mo (IV) oxide as an intermediate in the reduction process of MoO_4^{2-}.

Table 5. Elemental composition of Ni and Ni-Mo metallic coatings as measured from EDX analysis.

Sample type	Elemental composition (%)		
	Ni	Mo	O
Pure Ni	99.36	-	0.64
Ni:Mo 10:1	81.41	10.79	7.80
Ni:Mo 5:1	74.41	17.94	7.65

The three-dimensional surface topography of different coatings was obtained by AFM at a scan rate of 1.00 Hz and scan dimensions of 5.0x5.0 μm as shown in Fig. 8. The surface roughness of different films was expressed as average deviation parameters, R_a. It represents the average height of irregularities perpendicular to the surface. For different films the value of R_a was 32.47, 45.08 and 74.66 nm for pure Ni, Ni:Mo 10:1 and Ni:Mo 5:1, respectively. The effect of increase roughness of the Ni:Mo 5:1 is also indicated by the cathodic polarization curves [28].

4. CONCLUSIONS

1. Absorption spectra of Ni^{2+}, MoO_4^{2-}, glycinate ions showed some type of complexation as revealed from the change in the peak intensities and wavelengths.
2. XRD spectra revealed that, the increasing in Mo content in the metallic coating led to a decrease in the relative intensities and d-values of different orientations.
3. The corrosion resistance of the nanostructured coating increased with increasing the Mo content in the alloy.
4. The surface of metallic coating is relatively compact and smooth in case of pure Ni and Ni:Mo 10:1 while it is aggregated clusters in case of Ni:Mo 5:1.
5. The surface roughness of the metallic coating increased with increasing the Mo content in the alloy.

ACKNOWLEDGEMENT
This work was made possible by NPRP Grant 4-306-2-111 from the Qatar National Research Fund (a Member of The Qatar Foundation). The statements made herein are solely the responsibility of the authors.

References

1. R. Abdel-Karim, J. Halim, S. El-Raghy, M. Nabil, A. Waheed, *J. Alloys Comp*. 530 (2012) 85.
2. E. Beltowska-Lehman, P. Indyka, *Thin Solid Films* 520 (2012) 2046.
3. J.F. Kriz, H. Shimada, Y. Yoshimura, N. Matsubayashi, A. Nishijima, *Fuel* 74 (1995) 1852.
4. V.V. Kuznetsov, M.R. Pavlov, K.V. Kuznetsov, N. Kudryavtsev, *Russ. J. of Electrochem*. 39 (2003) 1338.
5. M. Donten, H. Cesiulis, Z. Stojek, *Electrochim. Acta* 50 (2005) 1405.
6. P. Kedzierzawski, D. Oleszak, M. Janik-Czachor, *Mater. Sci. Eng*. A 300 (2001) 105.
7. D. Oleszak, V.K. Portnoy, H. Matyja, *Mater. Sci. Forum* 312 (4) (1999) 345.
8. S.D. De la Torre, D. Oleszak, A. Kakitsuji, K. Miyaamoto, H. Miyamoto, R. Martinezm-S, F. Almeraya-C, A. Martinez-V, D. Rios-J, *Mater. Sci. Eng*. A 276 (2000) 226.
9. E.J. Podlaha, D. Landolt, *J. Electrochem. Soc*. 143 (3) (1996) 885.
10. E.J. Podlaha, D. Landolt, *J. Electrochem. Soc*. 144 (5) (1997) 1672.
11. K. Murase, M. Ogawa, T. Hirato, Y. Awakura, *J. Electrochem. Soc*. 151 (12) (2004) C798.
12. E. Gómez, E. Pellicer, E. Vallés, *J. Electroanal. Chem*. 580 (2005) 222.
13. E. Beltowska-Lehman, A. Bigos, P. Indyka, M. Kot, *Surf. Coat. Technol*. 211 (2012) 67.
14. T. Ohgai, Y. Tanaka, R. Washio, *J. Solid State Electrochem*. 17 (2013) 743.
15. S. Yagi, A. Kawakami, K. Murase, Y. Awakura, *Electrochim. Acta* 52 (2007) 6041.

16. C.C. Nee, W. Kim, R. Weil, *J. Electrochem. Soc*. 135 (5) (1988) 1100.
17. E. Uekawa, K. Murase, E. Matsubara, T. Hirato, Y. Awakura, *J. Electrochem. Soc*. 145 (1998) 523.
18. E. Chassaing, N. Portail, A.F. Levy, G. Wang, *J. Appl. Electrochem*. 34 (2004) 1085.
19. I. Rodriguez-Torres, G. Valentin, S. Chanel, F. Lapicque, Electrochim. Acta 46 (2000) 279.
20. A.E. Mohamed, S. M. Rashwan, S.M. Abdel-Wahaab, M.M. Kamel, J. Appl. Electrochem. 33 (2003) 1085.
21. S. M. Rashwan, A.E. Mohamed, S.M. Abdel-Wahaab, M.M. Kamel, J. Appl. Electrochem. 33 (2003) 1035.
22. S.H. Mosavat, M.E. Bahrololoom, M.H. Shariat, Appl. Surf. Sci. 257 (2011) 8311.
23. M. Chaudhury, J. Chem. Soc. Dalton Trans. (1983) 857.
24. M.R. Kidd, T.A. Chian, R. Dai, S. Zhang, J. Inorg. Biochem. 56 (1994) 213.
25. E. Gómez, E. Pellicer, E. Vallés, *J. Electroanal. Chem*. 517 (2001) 109.
26. S. Sun, E.J. Podlaha, *J. Electrochem. Soc.* 159 (2012) D97.
27. L.S. Sanches, S.H. Domingues, C.E.B. Marino, L.H. Mascaro, *Electrochem. Commun.* 6 (2004) 543.
28. J. Halim, R. Abdel-Karim, S. El-Raghy, M. Nabil, A. Waheed, *J. Nanomater.* 845673 (2012) 1.
29. M. Ebril, *Chim. Acta Turcica* 1 (1988) 59.
30. I. Dehri, H. Sozusaglam, M. Ebril., *Prog. Org. Coat*. 48 (2003) 118.
31. J.R. Macdonald (Ed.), 'Impedance Spectroscopy', John Wiley&Sons, New York, 1987, chapter 4.
32. A.S. Mogoda, Y.H. Ahmad, W.A. Badawy, *Mater. Chem. Phys*. 126 (2011) 676.
33. U. Rammelt, G. Reinhard, *Electrochim. Acta* 35 (1990) 1045.